





Active Earth Pressure Acting on Circular Shafts Using Numerical Approach

Abdelmajid Meftah ^{1*}, Naïma Benmebarek ², Sadok Benmebarek ²

¹ Department of Geographical Sciences and Topography, Constantine 1 University, P.O. Box, 325 Ain El Bey Way, Algeria.

² Department of Civil and Hydraulic Engineering, NMISSI Laboratory, Biskra University, BP 145 Biskra 07000, Algeria.

Received 28 December 2021; Revised 19 Marh 2022; Accepted 24 Marh 2022; Published 01 April 2022

Abstract

Retaining walls in axi-symmetric conditions and in plane strains have been widely treated in the literature using different approaches (limit equilibrium, limit analysis, slip line, and numerical techniques by finite elements or finite differences). The finite element or finite difference method provides more accurate solutions to the problem than the limit equilibrium method. In this paper, a new model of retaining wall in the axi-symmetry conditions under outward pressure is considered, this case can be widely used in the design of grain silos, buildings and road constructions. Numerical calculations using FLAC are reported to evaluate the evolution of the earth pressure distribution on a cylindrical wall filled with granular material and subjected to radial displacement. A parametric study is carried out in order to evaluate the distribution of the active earth pressure on the wall according to the radius, the angle of friction of the granular material, and the angle of friction of the interface granular material-wall. This study shows that there is an effect of the circular shape and the inclination of the wall on the active earth pressures.

Keywords: Earth Pressure; Axial Symmetry; Finite Difference Method; Slip Rate; Vertical Circular Retaining Wall.

1. Introduction

Determining the earth pressure acting on the well system is essential for its proper design. Several theoretical, experimental, and numerical methods have been proposed for the calculation of the active earth pressure on cylindrical retaining walls supporting aggregates. The theoretical methods are based on the theories provided by Coulomb (1776) [1] and Rankine (1857) [2]. Coulomb (1776) [1], was the first to propose the limit equilibrium method, and Prater (1977) [3], used it and adopted a Coulomb-type failure surface, which for axisymmetric conditions leads to a cone-shaped slippery mass. This same result was confirmed by Berezantzev (1958) [4], Chang and Hu (2005) [5], assuming a Rankine-type failure surface. Prater (1977) [3], concluded that there is a critical depth of a sink in purely cohesive soil ($c \neq 0$), regarding the passive earth pressure distribution, he concluded that passive pressure is linear with increasing excavation depth. Terzaghi (1943) [6], assumed a Rankine-type failure surface and a sliding mass in a cylindrical form, and concluded that the pressure is constant with the increasing excavation depth.

Keshavarz & Ebrahimi (2017) [7] used the slip line or Stress Characteristics Method (SCM) to analyze the active lateral earth pressure in the axi-symmetric case, The comparison of the results indicates the accuracy of the proposed method. For Tang (2020) [8], the footprint of a circular shaft is conducive to the engineering construction and avoids

* Corresponding author: abdelmadjid.meftah@umc.edu.dz

 <http://dx.doi.org/10.28991/CEJ-2022-08-04-09>



© 2022 by the authors. Licensee C.E.J, Tehran, Iran. This article is an open access article distributed under the terms and conditions of the Creative Commons Attribution (CC-BY) license (<http://creativecommons.org/licenses/by/4.0/>).

the unloading deformation effect of rectangular wells excavation, at the same time. Chehadeh et al. (2019) [9] show that the distance between the surcharge and the well wall was found to have a small effect on the magnitude of peak pressures. Contrary to what is observed under plane strain conditions, moreover, the theoretical estimated pressures underestimated the calculated values at greater depths and that the horizontal extent of the pressure propagation around the well was significantly influenced by the soil type as well as the width surcharge. Xiong et al. (2019) [10], presented a practical calculation formula for axisymmetric active earth pressure that is based on the linear superposition principle and the function fitting of pressure coefficients. The obtained solutions developed are demonstrated to be reasonably accurate compared with a set of experimental data obtained from the literature. According to Weidong et al. (2020) [11], the soil layer's active earth pressure near the top and bottom of the wall increases due to the soil arching, while the active earth pressure of the soil layer in the middle of the wall decreases relatively.

The experimental methods are based on the different modeling techniques of the excavation procedure for the implantation of a rigid, vertical and circular well in a granular soil. These techniques can be grouped into three groups: Push-in technique, adopted by Walz (1973) [12]. Temporary fluid pressure stabilization used by Lade et al. (1981) [13], who studied lateral earth pressure acting on flexible, circular and vertical wells. Fujii et al. (1994) [14], conducted centrifuge tests to study the effects of wall friction and soil displacements on the distribution of earth pressure around rigid wells. Based on the Distinct Element Method, three-dimensional calculations were carried out by Herten & Pulsfort (1999) [15], to determine the spatial earth pressure of sand on circular shaft constructions with respect to their deformation. Imamura et al. (1999) [16], developed a model tree similar to that used by Fujii et al. (1994) [14]. Chun & Shin (2006) [17], conducted model tests to study the effects of wall displacement and well size on earth pressure distribution as well as Tatiana & Mohamed (2011) [18], All of these researchers used a mechanically adjustable device shaft. Jaeyeon et al. (2015) [19], studied experimentally and numerically the arching effect on the active pressure by modifying the geometrical parameters of the well and the ground, they concluded that the arching effect on the lateral earth pressure is strongly dependent on the shaft diameter and height, angle of internal friction and soil cohesion value. Camber consists of transferring stresses around a region of the ground, which is then subjected to lower stresses (Paik & Salgado (2003) [20]). Xianfeng et al. (2021) [21], provided valuable insights for earth pressure distribution for design of circular deep shafts (e.g. 100 m) in using centrifuge tests in composite soil strata with clay and sand. They found that the lateral earth pressure of deep shaft in upper clay layer increases with depth, and the values are between active earth pressure and static earth pressure.

Most of the previous works consider that the earth pressure acts outside the circular wall. In this work, we propose a new model of retaining wall under the conditions of axi-symmetry. The wall is subjected to outward pressures which can be encountered widely in practice such as the design of grain silos. The numerical experiment is carried out using the FLAC software in order to evaluate the evolution of the earth pressure distribution on a cylindrical wall filled with granular material and subjected to a radial displacement [22]. A parametric study is carried out and the results of the two modes of internal and external axial symmetry are compared. A flowchart of the research methodology is employed in this study illustrated in Figure 1.

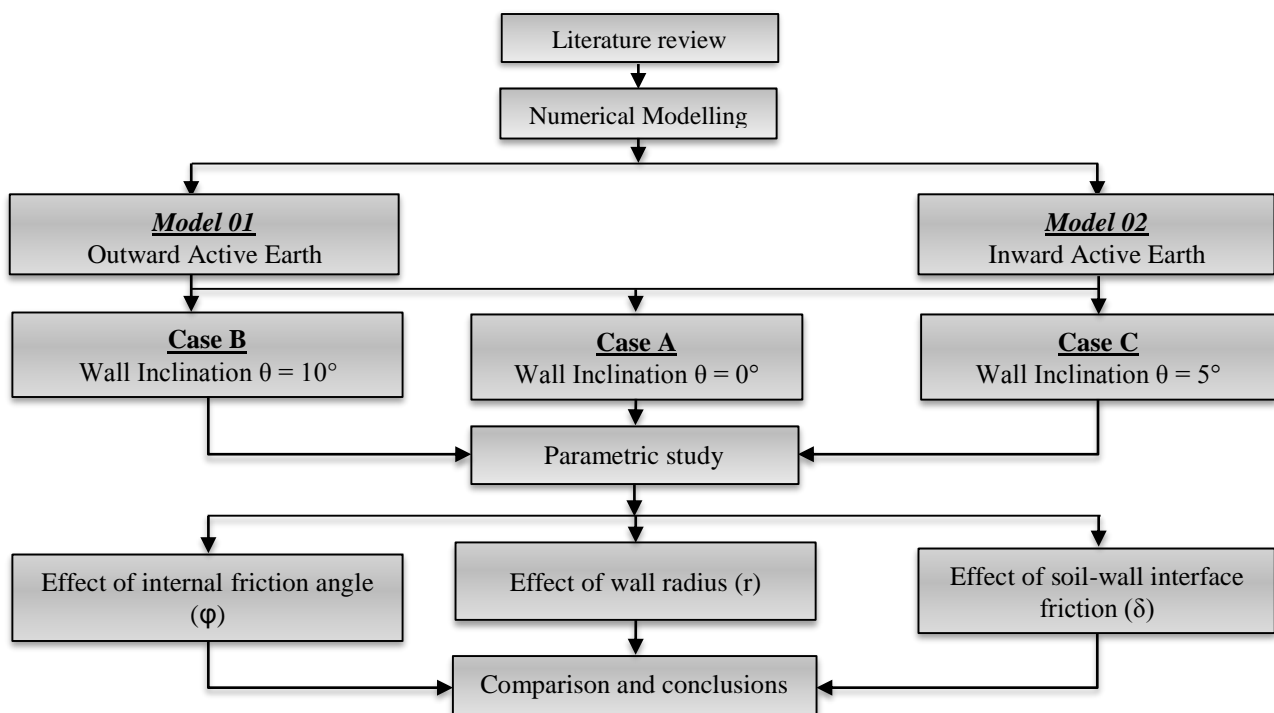


Figure 1. Research methodology flow chart

2. Numerical Modelling

2.1. Model Description

Two numerical models study was carried out by Finite Difference Method (FDM) using FLAC 2D. The two models were validated, parametric studies were conducted to obtain the evolution of the distribution of earth pressure on a cylindrical wall, and in all the case studies, the axi-symmetric conditions and the plane strain was adopted in the simulation. The proposed modeling procedure of the active earth pressure distribution on cylindrical shafts follows two steps:

- In the first one, the shaft installation and the geostatic stresses are computed assuming fixed shaft connected to the soil via interface element. At this stage the strength of the interface elements are assigned to be null and some stepping is required to bring the model to equilibrium;
- In the second step, a radial velocity towards the shaft axis was applied to the grid-points representing the wall shaft until a steady plastic flow is achieved (i.e. until a constant pressure on the shaft wall is reached). As the level of errors in such calculation scheme by FLAC depends on the applied velocity, a low velocity is recommended.

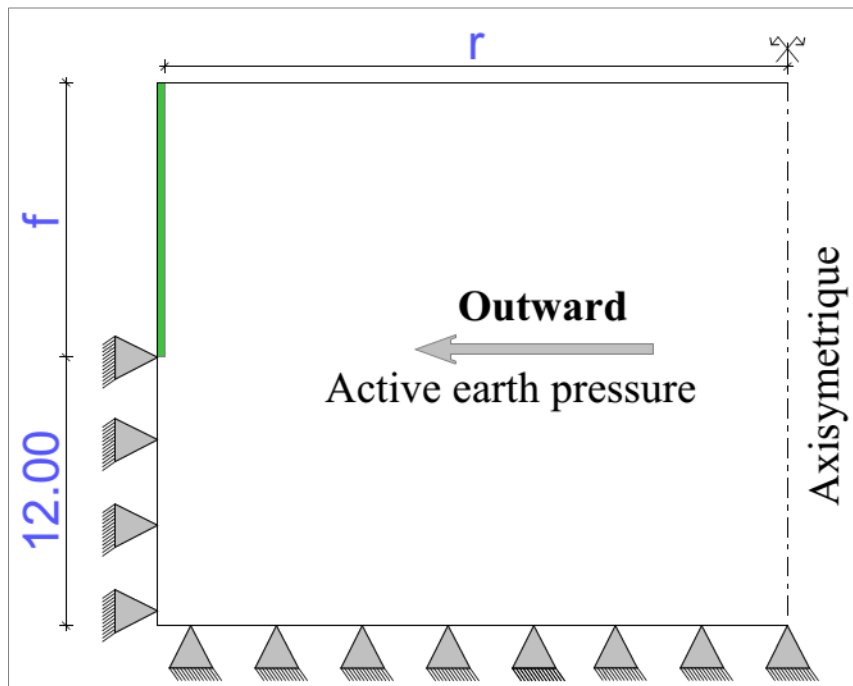


Figure 2. Retaining Walls in Axisymmetric Condition: Outward Mechanisms active earth pressure

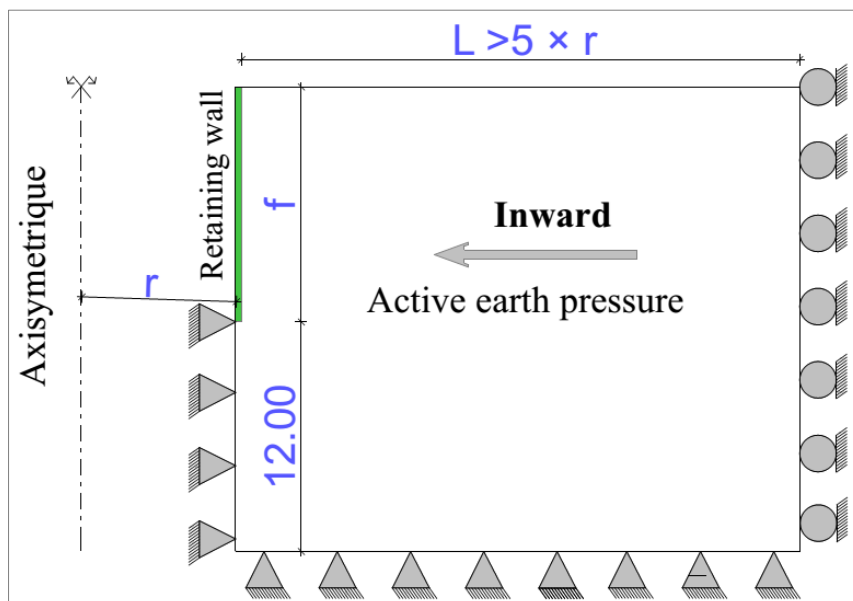


Figure 3. Retaining Walls in Axisymmetric Condition: Inward Mechanisms active earth pressure

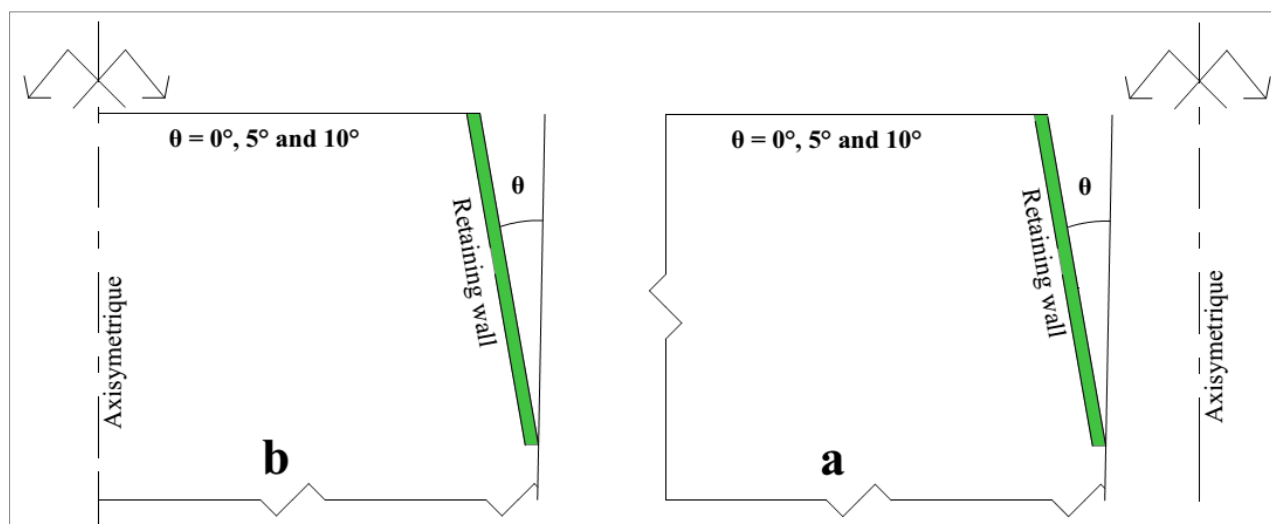


Figure 4. Geometry of the problem for (a) Inward and (b) outward retaining walls

2.2. Soil

The soil behavior is modeled by the elastic-perfectly plastic Mohr–Coulomb model encoded in FLAC code. The mesh size is fine near the wall where deformations are concentrated. Physical and mechanical characteristics assigned to the soil were: a shear modulus $G=11.25$ MPa, an elastic bulk modulus $K=30$ MPa internal friction angle $\varphi = 20^\circ, 25^\circ, 30^\circ, 35^\circ,$ and 40° , cohesion $c = 0$.

2.3. Boundary Conditions

As a general rule for the boundary conditions, the bottom boundary is assumed to be fixed in the two directions, the right and left lateral boundaries are fixed in the horizontal directions.

2.4. Structural Elements

Structural elements incorporated in FLAC do not support displacement loading. Therefore, the shaft wall is modelled by thin fixed membrane elements connected to the soil grid via interface elements attached on both sides.

2.5. Damping

The Mohr Coulomb model is an elastic-perfectly plastic model, in Geo Technologies this model is widely used in soil behavior modeling, in the elastic region of the stress-strain curve, the model behaves linearly and its deformations are determined based on Young and Poisson units. The failure criterion is determined by the friction angle (φ) and cohesion (c) of the soil.

2.6. Interface Elements

The elements of interface are used to represent the behavior of the zones of localization of the deformations in shear (slip surface) or in tension (cracks). Interface element at the contact surface of retaining walls and soil have been used.

3. Results and Discussions

The behavior of the ground is modeled by the elastic-perfectly plastic model of Mohr-Coulomb coded in FLAC code. All the following results are given for $\gamma=20$ kN/m³, bulk modulus $K = 30$ MPa, shear modulus $G = 11.25$ MPa, angle of internal friction $\varphi = 20^\circ, 25^\circ, 30^\circ, 35^\circ$ and 40° and cohesion $c = 0$.

3.1. Comparison with Other Studies

A comparison of the results of this study with those of the literature for plane and axisymmetric deformations is presented in Tables 1 to 3. Initially, for the inward and outward axisymmetric wall, the results (Table 1) of the axisymmetry of active earth pressure have been compared with those of Keshavarz & Ebrahimi (2017) [7], and those of plane strain of Coulomb (1773) [1]. The results show that the values obtained by the axisymmetric and for a large radius are slightly lower than those of the two studies but very close to the axisymmetric study.

Table 1. A comparison between the active earth pressure coefficients ($K_a\gamma$) in this study and other studies for the plane strain ($r = 1000\text{m}$, $c = 0$, $\gamma = 20 \text{ kN/m}^3$ and $\theta = 0^\circ$)

ϕ (deg.)	Keshavarz & Ebrahimi (2017) [7]		This study		Planestrain
	Inward	Outward	Inward	Outward	Coulomb (1773) [1]
10°	0.708	0.702	0.693	0.692	0.70
20°	0.491	0.487	0.464	0.462	0.49
30°	0.333	0.329	0.312	0.307	0.33

Secondly, for the axisymmetric inward wall and outward wall, the results of Tables 2 and 3 of the active earth pressure coefficients were compared with the plane strain results given by Coulomb (1997) [1], and those given by Soubra & Macuh (2002) [23]. As can be seen, when the radius of the wall increases from 100 to 1000 m, the values of the coefficients of the active lateral earth pressure of the axisymmetric case approach the case of plane strain but the difference increases with the internal friction angle in both cases. In outward case, the radius has no effect on earth pressure.

Table 2. A comparison between the active earth pressure coefficients for inward wall ($K_a\gamma$) in this study and other studies for the plane strain ($c = 0$, $\gamma = 20 \text{ kN/m}^3$ and $\theta = 0^\circ$)

ϕ (deg.)	Inward wall (this study)			Plane strain		
	δ (deg.)	$r_i = 100 \text{ m}$	$r_i = 1000 \text{ m}$	This study	Coulomb (1773) [1]	Soubra & Macuh (2002) [23]
20°	$\phi/3$	0.432	0.435	0.452	0.458	0.459
	$\phi/2$	0.417	0.419	0.435	0.437	0.442
30°	$\phi/3$	0.286	0.289	0.301	0.308	0.333
	$\phi/2$	0.273	0.281	0.292	0.297	0.303
40°	$\phi/2$	0.180	0.182	0.194	0.202	0.220
	$\phi/3$	0.180	0.181	0.192	0.199	0.202

Table 3. A comparison between the active earth pressure coefficients for outward wall ($K_a\gamma$) in this study and other studies for the plane strain ($c = 0$, $\gamma = 20 \text{ kN/m}^3$ and $\theta = 0^\circ$)

ϕ (deg.)	Outward wall (this study)			Plane strain		
	δ (deg.)	$r_i = 100 \text{ m}$	$r_i = 1000 \text{ m}$	This study	Coulomb (1773) [1]	Soubra & Macuh (2002) [23]
20°	$\phi/3$	0.435	0.433	0.452	0.458	0.459
	$\phi/2$	0.419	0.418	0.435	0.437	0.442
30°	$\phi/3$	0.287	0.286	0.301	0.308	0.333
	$\phi/2$	0.279	0.275	0.292	0.297	0.303
40°	$\phi/2$	0.179	0.180	0.194	0.202	0.220
	$\phi/3$	0.178	0.180	0.192	0.199	0.202

3.2. Implication and Explanation of Findings

In this part, we calculate and compare the active earth pressure acting on circular wells in both inward and outward. This work can also be a useful reference for geotechnical engineers to solve axisymmetric problems instead of using plane strain and especially for the case inward.

The results of the parametric study from the numerical experimentation of the active earth pressure coefficients inward or outward the wall are summarized in Tables 4 to 7. Figures 5 to 22 present the effects of parameters such as the wall inclination (θ), soil friction angle (ϕ), soil-wall interface angle (δ) and retaining wall radius (r), on active earth pressure coefficients, the radius has been plotted in a semi-logarithmic scale.

- The inclination of the wall (θ) varies from 0 to 10 degrees,
- The ground friction angle (ϕ) varies from 20 to 40 degrees
- The angle of the floor-wall interface (δ) varies from $\phi/3$, $\phi/2$, $2\phi/3$ to ϕ
- Radius of retaining wall (r) varies from 3 to 1000 m.

Table 4. Active earth pressure coefficients K_{ay} for axisymmetric Inward cases ($\theta = 0^\circ$)

φ	δ	r/f										
		1	1.5	2	2.5	3	3.5	4	4.5	5	33.33	333.33
20°	$\varphi/3$	0.369	0.387	0.398	0.405	0.410	0.414	0.416	0.419	0.420	0.432	0.435
	$\varphi/2$	0.361	0.378	0.389	0.396	0.401	0.405	0.408	0.410	0.411	0.423	0.426
	$2\varphi/3$	0.356	0.372	0.383	0.390	0.395	0.399	0.401	0.403	0.405	0.417	0.419
	φ	0.352	0.368	0.379	0.386	0.391	0.394	0.397	0.399	0.401	0.413	0.415
25°	$\varphi/3$	0.284	0.304	0.316	0.323	0.328	0.332	0.335	0.337	0.339	0.349	0.352
	$\varphi/2$	0.278	0.298	0.309	0.316	0.321	0.325	0.328	0.330	0.332	0.341	0.344
	$2\varphi/3$	0.274	0.294	0.305	0.312	0.317	0.321	0.223	0.326	0.327	0.337	0.340
	φ	0.275	0.295	0.306	0.313	0.318	0.322	0.325	0.327	0.328	0.339	0.341
30°	$\varphi/3$	0.217	0.236	0.247	0.254	0.259	0.262	0.265	0.267	0.269	0.286	0.289
	$\varphi/2$	0.213	0.232	0.242	0.249	0.254	0.257	0.260	0.262	0.264	0.276	0.283
	$2\varphi/3$	0.211	0.230	0.240	0.247	0.252	0.255	0.258	0.260	0.262	0.273	0.281
	φ	0.216	0.235	0.246	0.253	0.258	0.262	0.265	0.267	0.268	0.285	0.287
35°	$\varphi/3$	0.164	0.182	0.191	0.198	0.202	0.205	0.208	0.210	0.211	0.228	0.231
	$\varphi/2$	0.162	0.179	0.189	0.195	0.199	0.202	0.205	0.207	0.208	0.224	0.227
	$2\varphi/3$	0.162	0.179	0.189	0.195	0.199	0.202	0.205	0.207	0.208	0.224	0.227
	φ	0.168	0.187	0.197	0.203	0.208	0.211	0.214	0.216	0.218	0.236	0.237
40°	$\varphi/3$	0.122	0.138	0.147	0.152	0.156	0.159	0.161	0.163	0.164	0.180	0.182
	$\varphi/2$	0.121	0.136	0.145	0.150	0.154	0.157	0.159	0.161	0.162	0.178	0.180
	$2\varphi/3$	0.122	0.137	0.146	0.151	0.155	0.158	0.160	0.162	0.163	0.180	0.181
	φ	0.130	0.146	0.156	0.162	0.166	0.169	0.172	0.174	0.175	0.193	0.194

Table 5. Active earth pressure coefficients K_{ay} for axisymmetric Inward cases ($\theta = 5^\circ$)

φ	δ	r/f										
		1	1.5	2	2.5	3	3.5	4	4.5	5	33.33	333.33
20°	$\varphi/3$	0.356	0.375	0.386	0.392	0.397	0.400	0.403	0.405	0.407	0.417	0.419
	$\varphi/2$	0.351	0.369	0.380	0.386	0.391	0.394	0.397	0.399	0.401	0.412	0.413
	$2\varphi/3$	0.348	0.366	0.377	0.383	0.388	0.391	0.394	0.396	0.397	0.407	0.409
	φ	0.349	0.367	0.378	0.384	0.389	0.392	0.395	0.397	0.399	0.409	0.411
25°	$\varphi/3$	0.271	0.290	0.300	0.307	0.312	0.315	0.318	0.321	0.322	0.332	0.335
	$\varphi/2$	0.268	0.286	0.297	0.303	0.308	0.312	0.315	0.317	0.318	0.329	0.331
	$2\varphi/3$	0.267	0.285	0.296	0.302	0.307	0.310	0.313	0.315	0.317	0.327	0.330
	φ	0.272	0.291	0.302	0.309	0.313	0.317	0.320	0.322	0.324	0.334	0.336
30°	$\varphi/3$	0.205	0.222	0.232	0.238	0.243	0.246	0.249	0.251	0.252	0.269	0.272
	$\varphi/2$	0.203	0.221	0.230	0.237	0.241	0.244	0.247	0.249	0.250	0.267	0.270
	$2\varphi/3$	0.204	0.222	0.231	0.237	0.242	0.245	0.248	0.250	0.251	0.268	0.270
	φ	0.213	0.232	0.242	0.248	0.253	0.257	0.260	0.261	0.263	0.280	0.283
35°	$\varphi/3$	0.154	0.170	0.178	0.184	0.188	0.191	0.193	0.195	0.195	0.212	0.215
	$\varphi/2$	0.153	0.169	0.177	0.183	0.187	0.190	0.192	0.194	0.195	0.211	0.214
	$2\varphi/3$	0.155	0.171	0.180	0.186	0.189	0.192	0.195	0.196	0.197	0.214	0.216
	φ	0.167	0.184	0.193	0.200	0.204	0.207	0.210	0.211	0.213	0.230	0.233
40°	$\varphi/3$	0.113	0.127	0.134	0.139	0.143	0.145	0.147	0.149	0.149	0.164	0.166
	$\varphi/2$	0.114	0.127	0.135	0.140	0.143	0.146	0.148	0.150	0.150	0.165	0.167
	$2\varphi/3$	0.116	0.130	0.138	0.143	0.146	0.149	0.152	0.153	0.154	0.169	0.171
	φ	0.128	0.144	0.153	0.158	0.162	0.165	0.169	0.170	0.171	0.189	0.191

Table 6. Active earth pressure coefficients K_{ay} for axisymmetric Inward cases ($\theta = 10^\circ$)

φ	δ	r/f										
		1	1.5	2	2.5	3	3.5	4	4.5	5	33.33	333.33
20°	$\varphi/3$	0.346	0.364	0.373	0.380	0.384	0.388	0.390	0.392	0.394	0.404	0.406
	$\varphi/2$	0.343	0.360	0.370	0.377	0.381	0.384	0.387	0.389	0.390	0.400	0.402
	2 $\varphi/3$	0.341	0.359	0.369	0.375	0.379	0.383	0.385	0.387	0.389	0.399	0.401
	φ	0.345	0.363	0.372	0.379	0.383	0.386	0.389	0.391	0.393	0.403	0.405
25°	$\varphi/3$	0.262	0.279	0.289	0.295	0.300	0.303	0.306	0.308	0.310	0.319	0.323
	$\varphi/2$	2.260	0.277	0.287	0.294	0.298	0.301	0.304	0.306	0.308	0.318	0.321
	2 $\varphi/3$	0.261	0.278	0.288	0.294	0.299	0.302	0.305	0.307	0.309	0.318	0.322
	φ	0.269	0.286	0.297	0.303	0.308	0.311	0.314	0.316	0.318	0.328	0.330
30°	$\varphi/3$	0.196	0.212	0.221	0.227	0.231	0.234	0.237	0.239	0.240	0.256	0.259
	$\varphi/2$	0.196	0.212	0.221	0.227	0.231	0.234	0.237	0.239	0.240	0.256	0.259
	2 $\varphi/3$	0.199	0.215	0.224	0.230	0.234	0.237	0.240	0.242	0.243	0.259	0.261
	φ	0.210	0.227	0.236	0.243	0.247	0.250	0.253	0.255	0.256	0.274	0.276
35°	$\varphi/3$	0.146	0.160	0.168	0.173	0.176	0.179	0.181	0.183	0.184	0.199	0.203
	$\varphi/2$	0.147	0.161	0.169	0.174	0.178	0.180	0.183	0.184	0.185	0.201	0.204
	2 $\varphi/3$	0.150	0.165	0.173	0.178	0.182	0.184	0.187	0.188	0.189	0.206	0.208
	φ	0.163	0.179	0.189	0.193	0.197	0.200	0.203	0.204	0.205	0.223	0.226
40°	$\varphi/3$	0.107	0.119	0.126	0.130	0.133	0.135	0.137	0.138	0.139	0.153	0.156
	$\varphi/2$	0.109	0.121	0.128	0.132	0.135	0.137	0.139	0.141	0.142	0.156	0.158
	2 $\varphi/3$	0.112	0.125	0.132	0.137	0.140	0.142	0.144	0.145	0.146	0.161	0.163
	φ	0.126	0.140	0.148	0.154	0.157	0.159	0.162	0.163	0.164	0.181	0.184

Table 7. Active earth pressure coefficients K_{ay} for axisymmetric Outward

φ	δ	$\theta = 0^\circ$			$\theta = 5^\circ$			$\theta = 10^\circ$		
		r/f			r/f			r/f		
		2.5	33.33	333.33	2.5	33.33	333.33	2.5	33.33	333.33
20°	$\varphi/3$	0.435	0.435	0.433	0.417	0.418	0.417	0.403	0.406	0.405
	$\varphi/2$	0.425	0.425	0.424	0.410	0.412	0.412	0.398	0.402	0.401
	2 $\varphi/3$	0.418	0.419	0.418	0.406	0.409	0.409	0.395	0.400	0.400
	φ	0.412	0.414	0.415	0.405	0.410	0.410	0.397	0.404	0.403
25°	$\varphi/3$	0.352	0.351	0.347	0.334	0.334	0.330	0.315	0.322	0.318
	$\varphi/2$	0.343	0.344	0.340	0.326	0.330	0.327	0.312	0.320	0.316
	2 $\varphi/3$	0.339	0.339	0.336	0.323	0.329	0.326	0.312	0.321	0.317
	φ	0.338	0.340	0.338	0.328	0.335	0.333	0.321	0.330	0.327
30°	$\varphi/3$	0.288	0.287	0.286	0.268	0.268	0.269	0.255	0.256	0.256
	$\varphi/2$	0.276	0.274	0.274	0.267	0.266	0.267	0.255	0.256	0.256
	2 $\varphi/3$	0.280	0.279	0.275	0.267	0.267	0.268	0.257	0.257	0.259
	φ	0.285	0.286	0.282	0.278	0.279	0.281	0.270	0.268	0.271
35°	$\varphi/3$	0.230	0.230	0.228	0.212	0.210	0.212	0.200	0.201	0.200
	$\varphi/2$	0.227	0.227	0.225	0.211	0.210	0.207	0.201	0.202	0.202
	2 $\varphi/3$	0.226	0.227	0.225	0.214	0.212	0.214	0.205	0.205	0.206
	φ	0.236	0.238	0.235	0.229	0.228	0.231	0.221	0.220	0.224
40°	$\varphi/3$	0.182	0.179	0.180	0.165	0.162	0.165	0.154	0.151	0.155
	$\varphi/2$	0.180	0.177	0.179	0.166	0.160	0.166	0.157	0.157	0.156
	2 $\varphi/3$	0.181	0.178	0.180	0.168	0.166	0.169	0.161	0.160	0.163
	φ	0.195	0.191	0.193	0.185	0.185	0.188	0.179	0.177	0.181

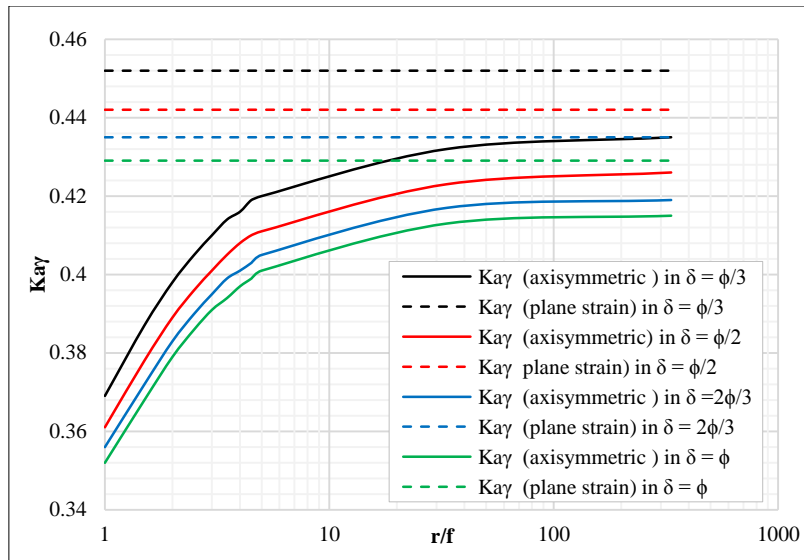


Figure 5. Active earth pressure coefficients for Axisymmetric Inward in $\phi = 20^\circ$ and $\theta = 0^\circ$

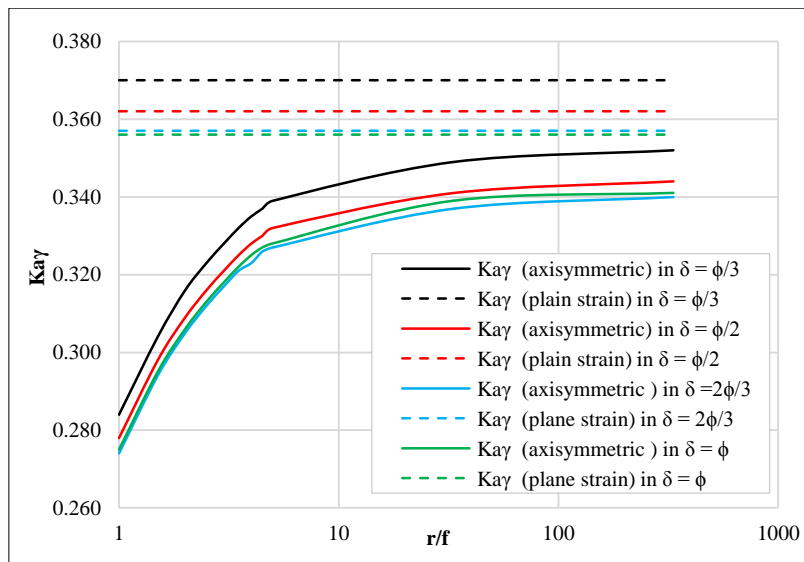


Figure 6. Active earth pressure coefficients for Axisymmetric Inward in $\phi = 25^\circ$ and $\theta = 0^\circ$

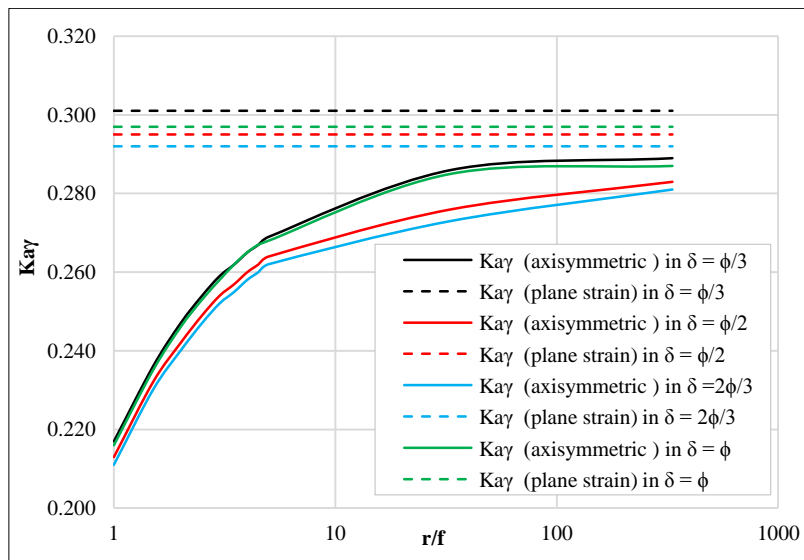


Figure 7. Active earth pressure coefficients for Axisymmetric Inward in $\phi = 30^\circ$ and $\theta = 0^\circ$

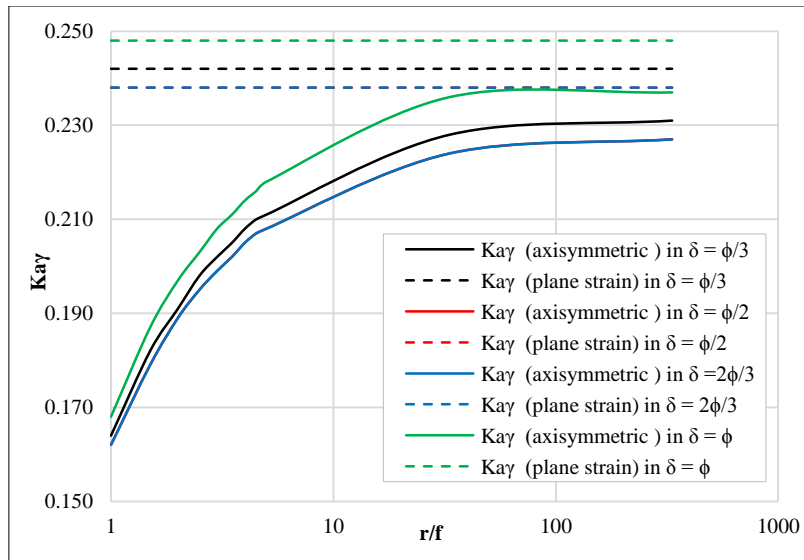


Figure 8. Active earth pressure coefficients for Axisymmetric Inward in $\phi = 35^\circ$ and $\theta = 0^\circ$

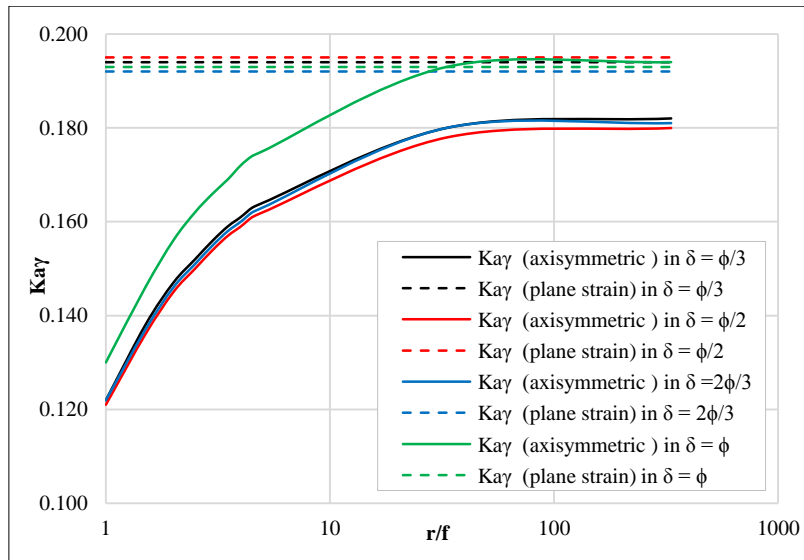


Figure 9. Active earth pressure coefficients for Axisymmetric Inward in $\phi = 40^\circ$ and $\theta = 0^\circ$

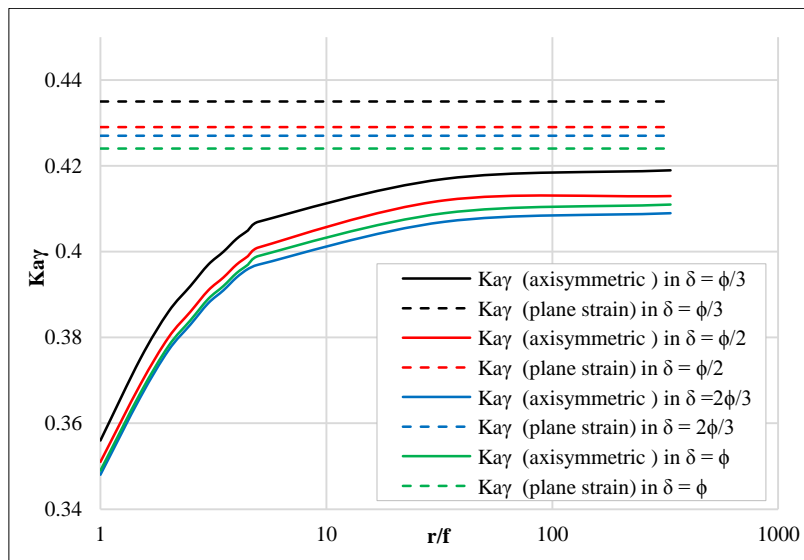


Figure 10. Active earth pressure coefficients for Axisymmetric Inward in $\phi = 20^\circ$ and $\theta = 5^\circ$

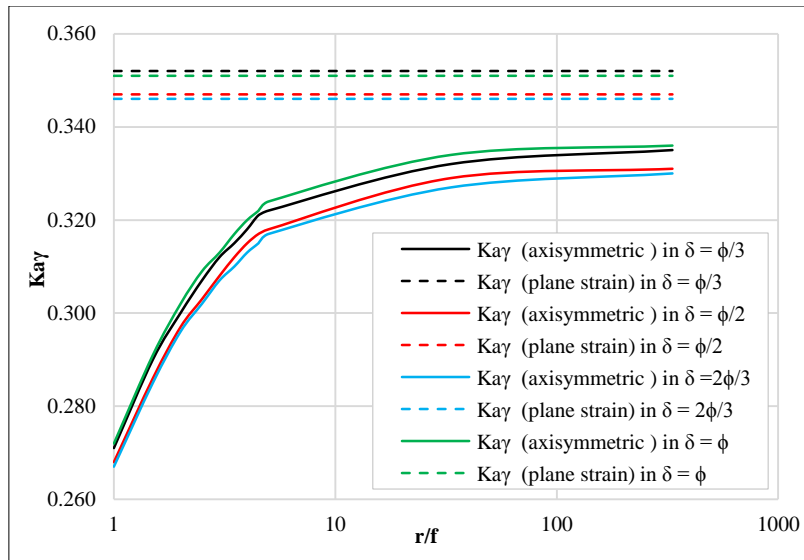


Figure 11. Active earth pressure coefficients for Axisymmetric Inward in $\phi = 25^\circ$ and $\theta = 5^\circ$

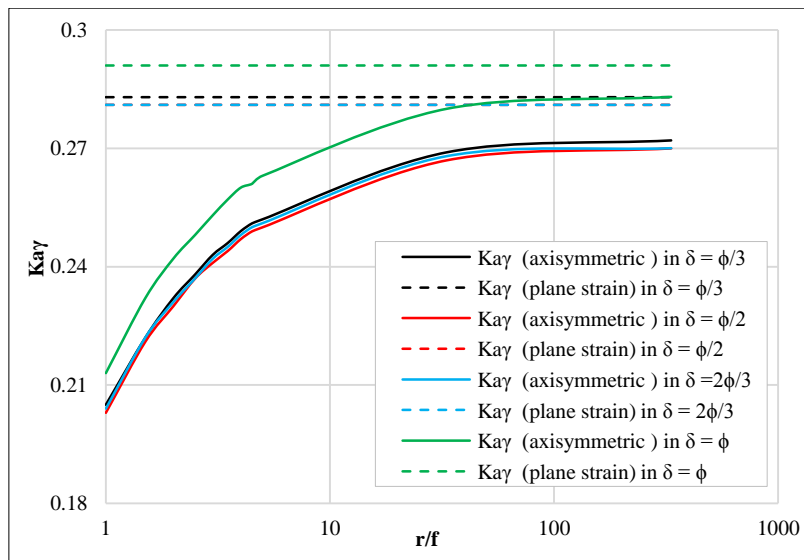


Figure 12. Active earth pressure coefficients for Axisymmetric Inward in $\phi = 30^\circ$ and $\theta = 5^\circ$

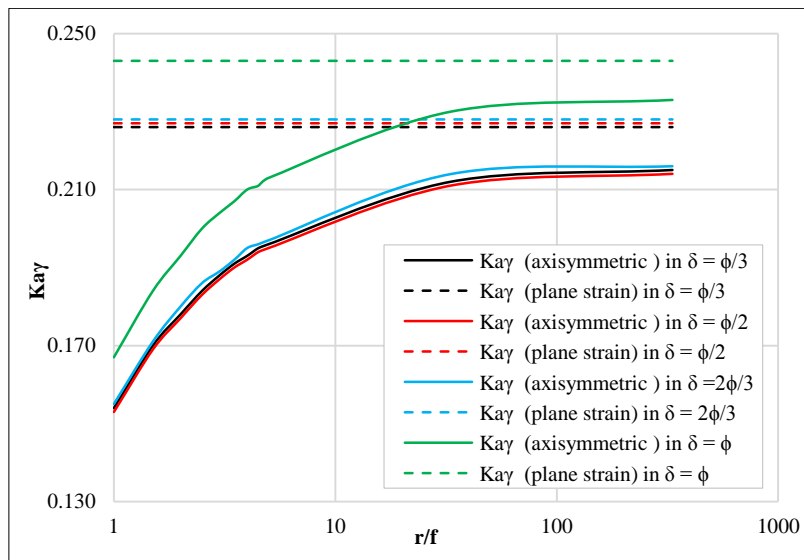


Figure 13. Active earth pressure coefficients for Axisymmetric Inward in $\phi = 35^\circ$ and $\theta = 5^\circ$

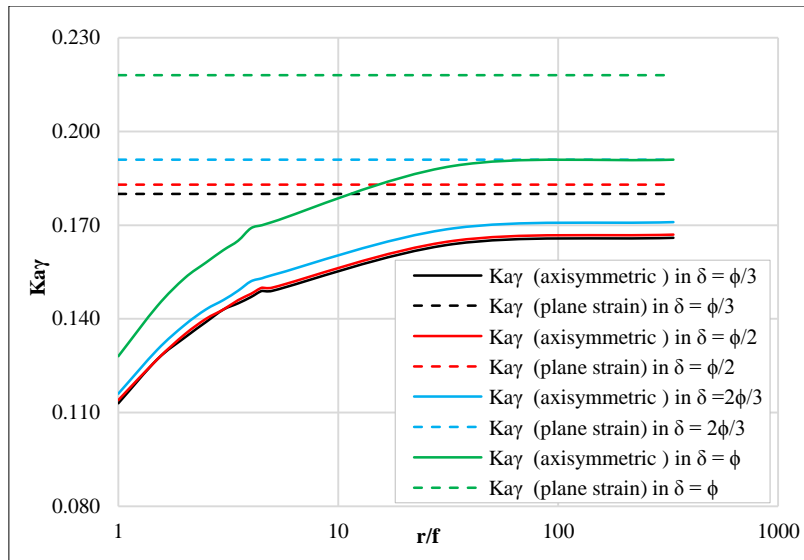


Figure 14. Active earth pressure coefficients for Axisymmetric Inward in $\phi = 40^\circ$ and $\theta = 5^\circ$

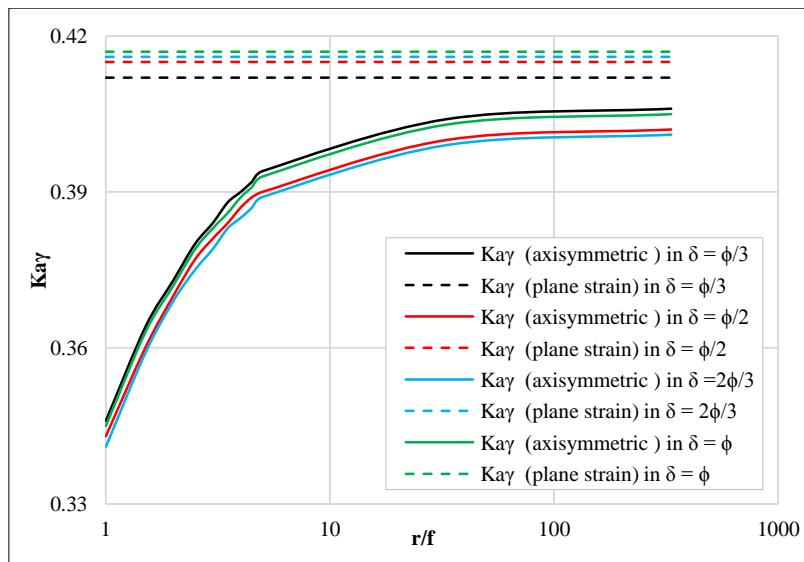


Figure 15. Active earth pressure coefficients for Axisymmetric Inward in $\phi = 20^\circ$ and $\theta = 10^\circ$

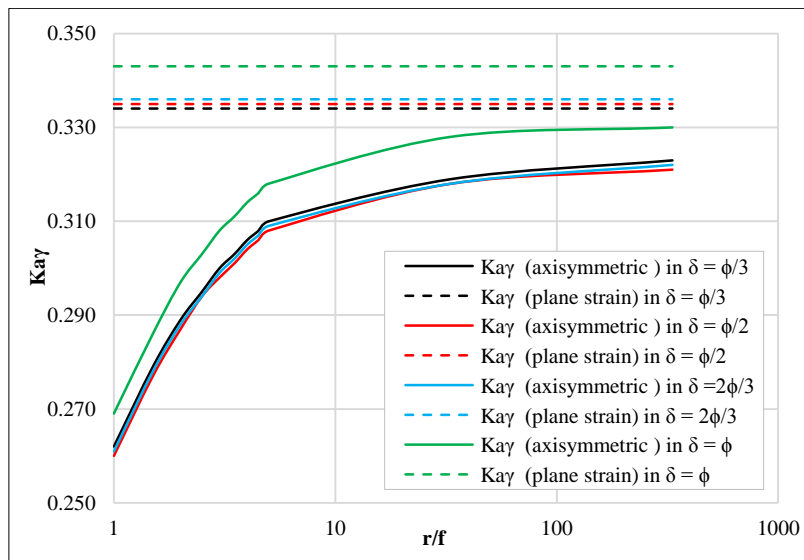


Figure 16. Active earth pressure coefficients for Axisymmetric Inward in $\phi = 25^\circ$ and $\theta = 10^\circ$

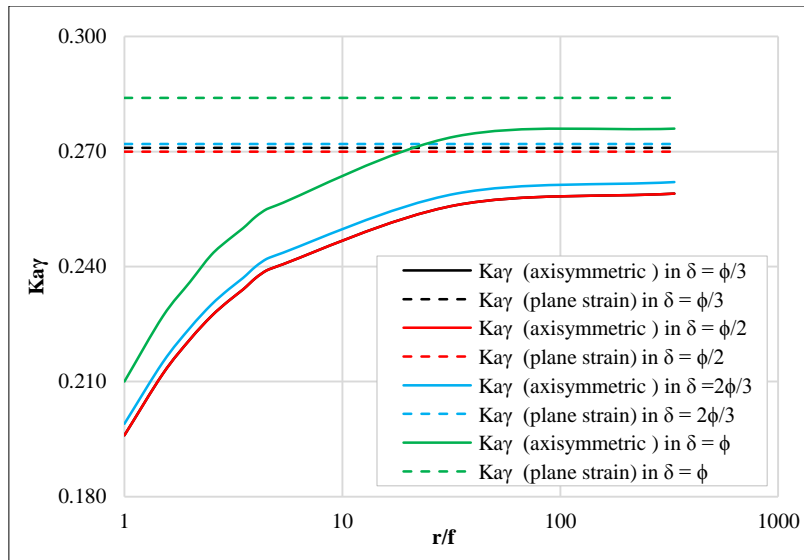


Figure 17. Active earth pressure coefficients for Axisymmetric Inward in $\phi = 30^\circ$ and $\theta = 10^\circ$

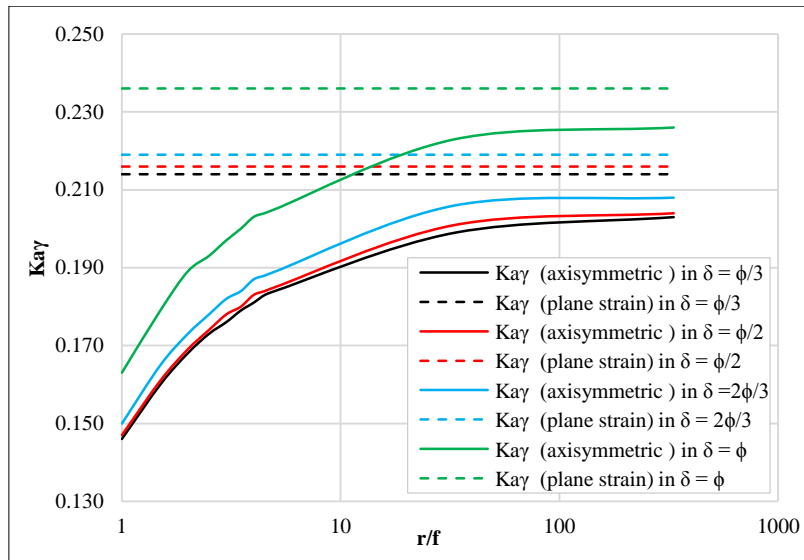


Figure 18. Active earth pressure coefficients for Axisymmetric Inward in $\phi = 35^\circ$ and $\theta = 10^\circ$

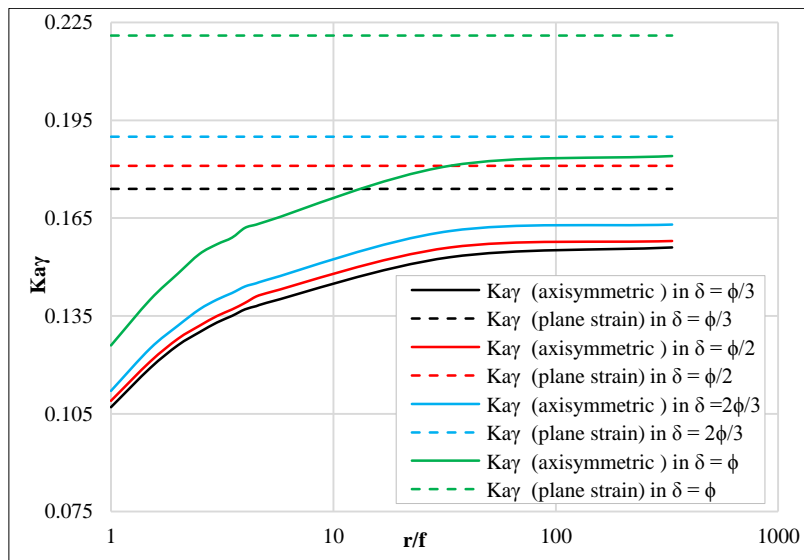


Figure 19. Active earth pressure coefficients for Axisymmetric Inward $\phi = 40^\circ$ and $\theta = 10^\circ$

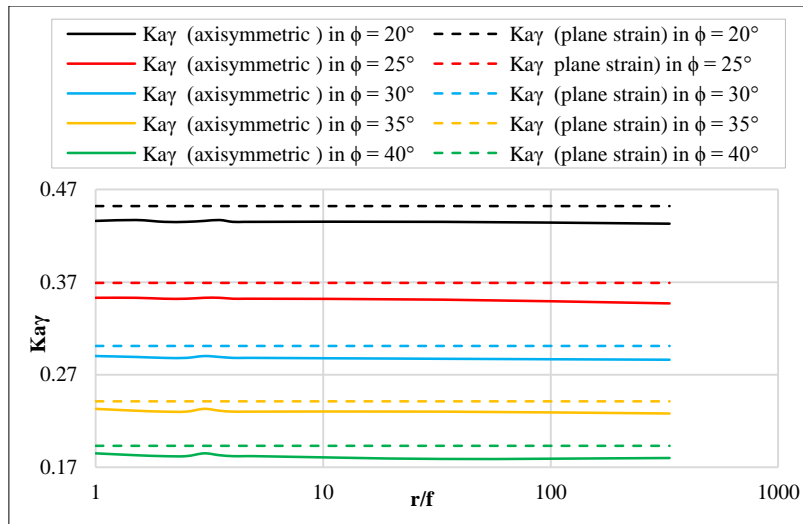


Figure 20. Active earth pressure coefficients for Axisymmetric Outward in $\delta = 2\phi/3$ and $\theta = 0^\circ$

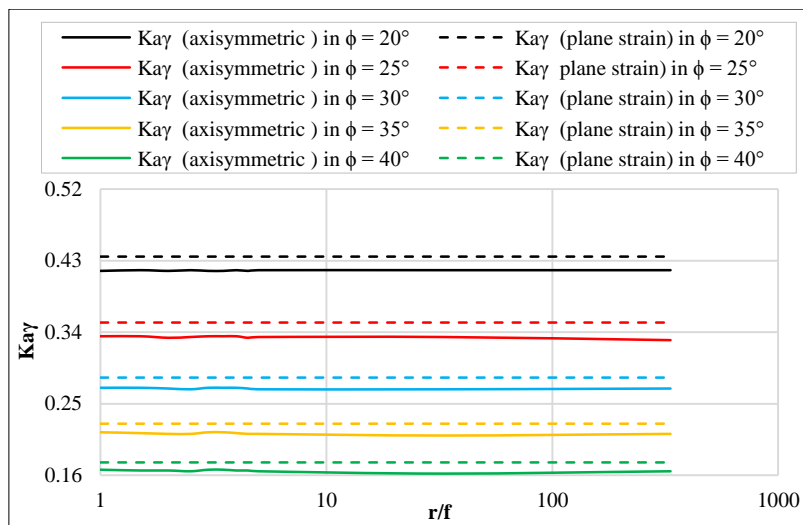


Figure 21. Active earth pressure coefficients for Axisymmetric Outward $\delta = 2\phi/3$ and $\theta = 5^\circ$

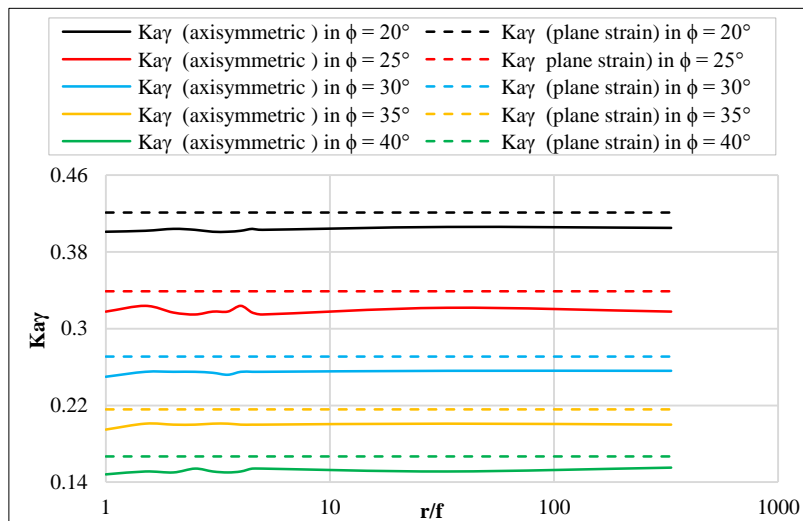


Figure 22. Active earth pressure coefficients for Axisymmetric Outward in $\delta = 2\phi/3$ and $\theta = 10^\circ$

Figures 5 to 22 and Tables 4 to 7 show that for both cases:

- The coefficient of the active earth pressure decreases with the internal soil friction angle ϕ and the dilatancy angle (θ).
- Contrary to the parameters (θ , ϕ and r), the increase in wall friction has a non-constant effect on the active earth

pressure coefficients. Indeed, the coefficient of the active earth pressure decreases with the angle of the soil-wall interface (δ) for an angle φ of 20° whereas as the angle δ increases the coefficient K_{ay} increases. Especially for a rough surface of the wall ($\varphi = \delta$).

For inward wall:

- The radius has a remarkable effect on active earth pressure. The curves 5 to 19 clearly show that the earth pressure coefficient increases with the radius and tends towards a plateau for considerable radii $r/f > 340$.
- For very large radii, the earth pressure coefficient in axis-symmetry approaches those of the plane case but with lower values

For outward wall:

- The radius appears to have no effect on active earth pressure (Figures 20 to 22). The part of the ground mobilized by the earth pressure is free and is not influenced by the interior.
- The values of the earth pressure coefficients in axis-symmetry seem slightly lower than those of plane strain.

The comparison between the two cases shows that for very large radii, the earth pressure distribution is identical and that the difference appears at the bottom of the wall. The inward active pressure stress is slightly lower for non-expanding soils ($\theta = 0^\circ$) but becomes higher for expanding soils ($\theta \neq 0^\circ$) (Figure 23).

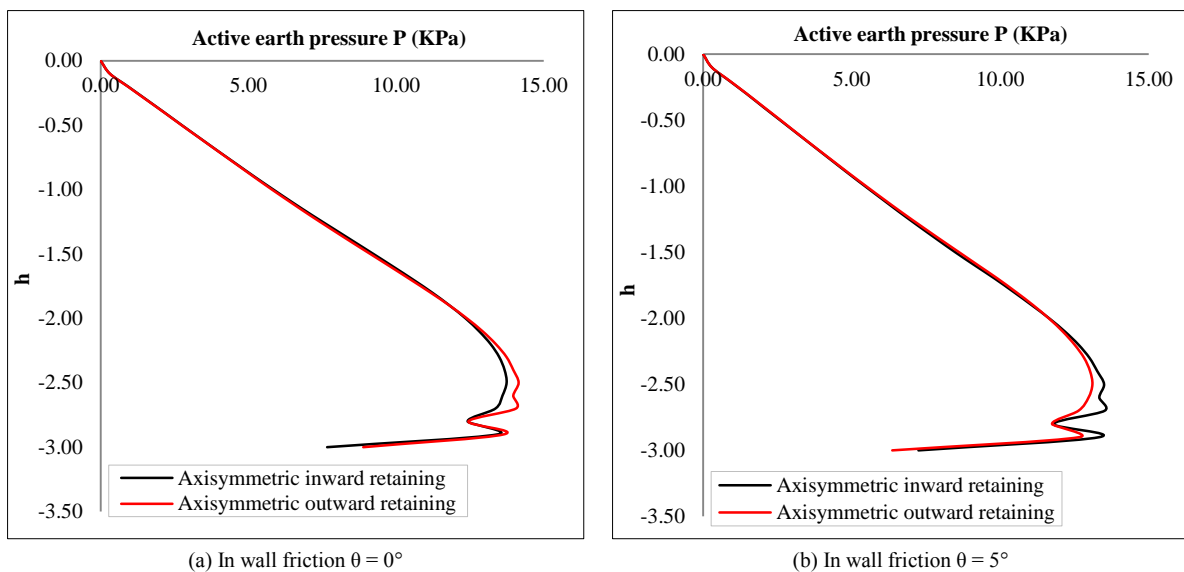


Figure 23. Comparison of the active earth pressure distribution ($\varphi = 30^\circ$, $\delta = \varphi/3$ and $r/f=333.33$)

For small radii, the shape of the active earth stress distribution curves is the same in both cases and the outward stresses are significantly greater than the inward stresses except at the top of the wall (Figures 24 and 25).

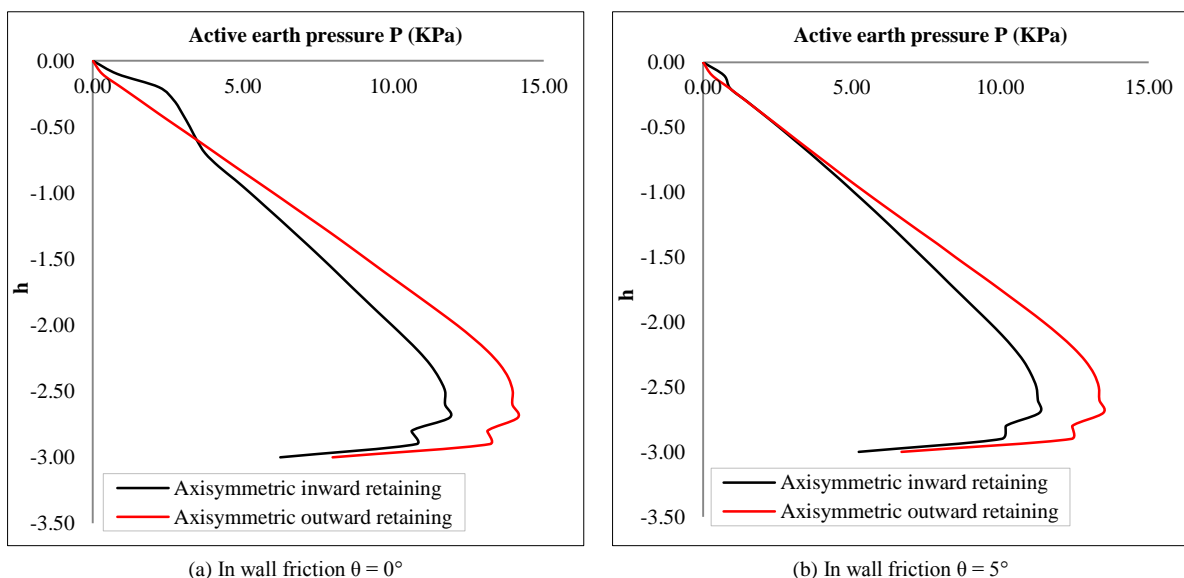


Figure 24. Comparison of the active earth pressure distribution ($\varphi = 30^\circ$, $\delta = \varphi/3$ and $r/f = 2$)

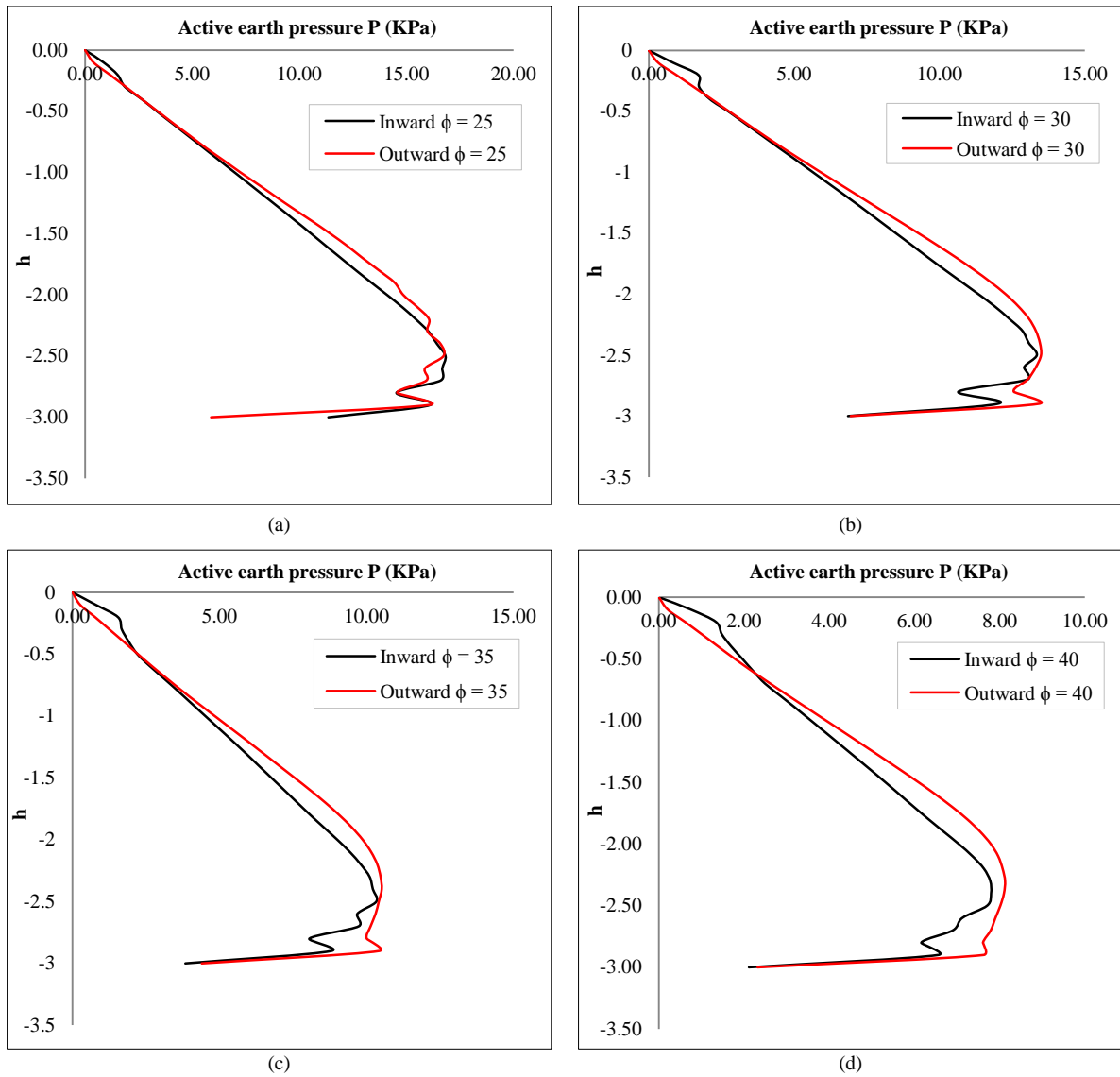


Figure 25. Comparison of the active earth pressure distribution ($\delta = \phi/3$, $\theta = 0^\circ$ and $r/f = 5$)

The effect of the interface on the distribution of active earth stresses is identical in both cases for a very large radius from the point of view of shape and values (Figure 26).

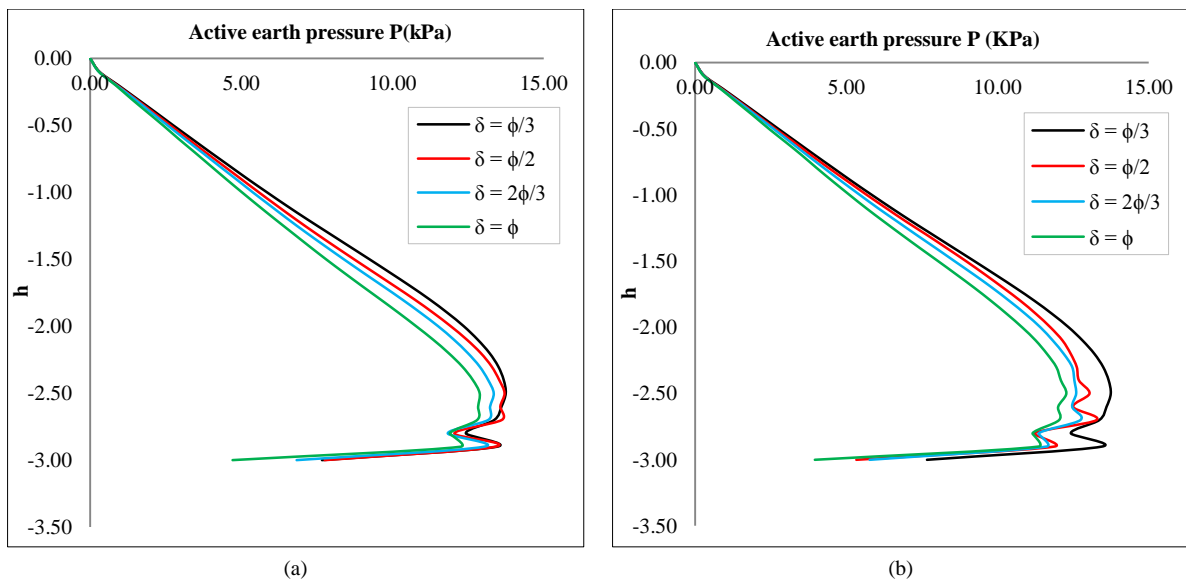


Figure 26. The effect of the wall friction angle on the distributions of the lateral earth pressure for the cases of (a) inward and (b) outward ($\phi = 30^\circ$ and $\theta = 0^\circ$ and $r/f = 334$)

4. Conclusions

This study evaluated the axisymmetric active lateral earth pressure of the retaining wall using the explicit finite difference code FLAC (Fast Lagrangian Continuum Analysis). Before starting numerical experiments, three types of retaining walls in the axisymmetric case were considered. The results of the chosen model were compared with those of the literature. The comparison showed good agreement. The results were presented and discussed in terms of earth pressures on the wall. The following conclusions were drawn as follows:

- There is an effect of the circular shape of the wall on the active earth pressures;
- The coefficient of axi-symmetric active earth pressures is lower than 2D active earth pressures;
- For the inward case, the active earth pressure increases with radius and tends to approach the coulomb value for very large radii;
- For the outward case, the coefficient of the active earth pressures does not depend on the radius and its value is identical to the other case (inward) for high radii because the part of the ground mobilized by the earth pressure is free and is not influenced by the interior;
- The coefficient of active earth pressure is the same in both cases (inward case and outward case) when the relative radius $r/f > 34$;
- The inclination of the wall also affects the coefficient, which decreases with increasing inclination angle in both cases.

4.1. Future Aspects of the Research

This work will be a starting point. Further research, such as calculation of the passive earth coefficient and effect of water flow, should be conducted to reduce the risk of failure of such structures.

5. Declarations

5.1. Author Contributions

Conceptualization, M.A.; writing—preparation of the original draft, M.A. and B.N.; writing—editing and editing, B.A.; B.N. and B.S. All authors have read and accepted the published version of the manuscript.

5.2. Data Availability Statement

The data presented in this study are available in the article.

5.3. Funding

The authors received no financial support for the research, authorship, and/or publication of this article.

5.4. Acknowledgements

The authors express their gratitude to the Directorate General for Scientific Research and Technological Development of Algeria.

5.5. Conflicts of Interest

The authors declare no conflict of interest.

6. References

- [1] Coulomb, C.A. (1776). Essay on an application of the rules of maximis and minimis to some problems of statics relating to architecture. *Memoirs of Mathematics and Physics, Presented to the Royal Academy of Sciences, by various Scholars, and read in its Assemblies, Paris, France, Vol. 7, 343–382. (In France).*
- [2] Rankine, W. J. M. (1857). II. On the stability of loose earth. *Philosophical Transactions of the Royal Society of London*, 147 (1 January 1857), 9–27. doi:10.1098/rstl.1857.0003.
- [3] Prater, E. G. (1977). Examination of Some Theories of Earth Pressure on Shaft Linings. *Canadian Geotechnical Journal*, 14(1), 91–106. doi:10.1139/t77-007.
- [4] Berezantzev, V. G. (1958). Earth pressure on the cylindrical retaining wall. *Proceedings Conference on Earth Pressure Problems, Butterworths, London, vol. 2, September 1958, 21–27.*
- [5] Cheng, Y. M., & Hu, Y. Y. (2005). Active earth pressure on circular shaft lining obtained by simplified slip line solution with general tangential stress coefficient. *Chinese Journal of Geotechnical Engineering*, 2005, 27: 110, 115.

- [6] Terzaghi, K. (1943). *Theoretical Soil Mechanics*. John Wiley & Son, Hoboken, United States. doi:10.1002/9780470172766.
- [7] Keshavarz, A., & Ebrahimi, M. (2017). Axisymmetric passive lateral earth pressure of retaining walls. *KSCE Journal of Civil Engineering*, 21(5), 1706-1716. doi:10.1007/s12205-016-0502-9.
- [8] Tang, Z. (2020). Design and Construction of the Circular Shape Shaft Using the Reverse Construction Method. In *E3S Web of Conferences* (Vol. 198, p. 02011). EDP Sciences. doi:10.1051/e3sconf/202019802011.
- [9] Chehadeh, A., Turan, A., Abed, F., & Yamin, M. (2019). Lateral earth pressures acting on circular shafts considering soil-structure interaction. *International Journal of Geotechnical Engineering*, 13(2), 139–151. doi:10.1080/19386362.2017.1328081.
- [10] Xiong, G. J., Wang, J. H., & Chen, J. J. (2019). Theory and practical calculation method for axisymmetric active earth pressure based on the characteristics method considering the compatibility condition. *Applied Mathematical Modelling*, 68, 563–582. doi:10.1016/j.apm.2018.11.022.
- [11] Hu, W., Liu, K., Zhu, X., Tong, X., & Zhou, X. (2020). Active Earth Pressure against Rigid Retaining Walls for Finite Soils in Sloping Condition considering Shear Stress and Soil Arching Effect. *Advances in Civil Engineering* (Vol. 2020). doi:10.1155/2020/6791301.
- [12] Walz, B. (1973). Apparatus for measuring the spatial earth pressure on a round model caisson. *Construction Machinery and Engineering*, 20, 339-344. (In France).
- [13] Lade, P. V., Jessberger, H. L., Makowski, E., & Jordan, P. (1981). Modeling of Deep Shafts in Centrifuge Tests. *Proceedings of the International Conference on Soil Mechanics and Foundation Engineering*, Stockholm, Sweden, vol. 1, 15-19 June 1981, 683–691. doi:10.1016/0148-9062(83)91480-8.
- [14] Fujii, T., Hagiwara, T., Ueno, K., & Taguchi, A. (1994). Experiment and analysis of earth pressure on an axisymmetric shaft in sand. *Proceedings of the International Conference Centrifuge 94*, Balkema Rotterdam, Netherlands, August 1994, 791–796.
- [15] Herten, M., & Pulsfort, M. (1999). Determination of spatial earth pressure on circular shaft constructions. *Granular Matter*, 2(1), 1–7. doi:10.1007/s100350050028.
- [16] Imamura, S., Nomoto, T., Fujii, T and Hagiwar, T. (2000). Earth pressures acting on a deep shaft and the movements of adjacent ground in sand. *Geotechnical Aspects of Underground Construction in Soft Ground*. Balkema, Rotterdam, Tokyo, Japan (July 1999): 647–652
- [17] Chun, B., & Shin, Y. (2006). Active earth pressure acting on the cylindrical retaining wall of a shaft. *Journal of the Korean GEO-environmental Society*, 7(4), 15-24.
- [18] Tobar, T., & Meguid, M. A. (2011). Experimental Study of the Earth Pressure Distribution on Cylindrical Shafts. *Journal of Geotechnical and Geoenvironmental Engineering*, 137(11), 1121–1125. doi:10.1061/(asce)gt.1943-5606.0000535.
- [19] Cho, J., Lim, H., Jeong, S., & Kim, K. (2015). Analysis of lateral earth pressure on a vertical circular shaft considering the 3D arching effect. *Tunnelling and Underground Space Technology*, 48, 11–19. doi:10.1016/j.tust.2015.01.002.
- [20] Paik, K. H., & Salgado, R. (2003). Estimation of active earth pressure against rigid retaining walls considering arching effects. *Geotechnique*, 53(7), 643–653. doi:10.1680/geot.2003.53.7.643.
- [21] Benmoussa, S., Benmebarek, S., & Benmebarek, N. (2021). Bearing Capacity Factor of Circular Footings on Two-layered Clay Soils. *Civil Engineering Journal*, 7(5), 775–785. doi:10.28991/cej-2021-03091689.
- [22] FLAC (2005). *Fast Lagrangian Analysis of Continua*. Vol. I, User's Manual, Vol. II. Verification Problems and Example Applications (2nd Edition) (FLAC3D Version 3.0), Minneapolis, Unites States.
- [23] Soubra, A. H., & Macuh, B. (2002). Active and passive earth pressure coefficients by a kinematical approach. *Proceedings of the Institution of Civil Engineers-Geotechnical Engineering*, 155(2), 119-131. doi:10.1680/geng.2002.155.2.119.